Earth Planet. Sci. Lett. 655 (2025) 119253

Contents lists available at ScienceDirect

Earth and Planetary Science Letters

journal homepage: www.elsevier.com/locate/epsl

Late Cenozoic intensification of deoxygenation in the Pacific Ocean

Katrina Nilsson-Kerr [a,b,*], Babette A.A. Hoogakker [a,*], Dharma A. Reyes Macaya [a,c], Helge A. Winkelbauer [a], Elliott Hamilton [d], Simon Chenery [d], Catherine V Davis [e], Melanie J. Leng [d]

[a] Lyell Centre, Heriot-Watt University, Edinburgh, UK
[b] Department of Earth Sciences, University of Bergen, and Bjerknes Centre for Climate Research, Bergen, Norway
[c] MARUM-Center for Marine Environmental Sciences, University of Bremen, Bremen, Germany
[d] British Geological Survey, Keyworth, Nottingham, UK
[e] Department of Marine, Earth, and Atmospheric Sciences, North Carolina State University, Raleigh, NC, USA

ARTICLE INFO

Keywords:
Paleoceanography
Cenozoic
Foraminifera
Geochemistry

ABSTRACT

The Pacific Ocean hosts the largest expanse of oxygen depleted waters owing to a combination of factors influencing oxygen supply and consumption, with consequences for biogeochemical cycling. However, understanding of the long-term evolution of the Pacific Oxygen Deficient Zone remains poorly constrained. Here we apply the Iodine to Calcium (I/Ca) ratio in planktic foraminifera, in combination with the absence/presence of *Globorotaloides hexagonus*, from four tropical Pacific Ocean sites to reconstruct oceanic oxygen across the late Cenozoic. To validate the application of I/Ca, we supplement existing I/Ca calibration datasets by expanding their spatial coverage with additional core-top measurements. Our downcore results, combined with other lines of evidence, indicate the emergence and establishment of low oxygen waters from the late Miocene-Pliocene. The decline in Pacific Ocean oxygen accompanies large-scale climate and tectonic changes and likely impacted marine carbon cycling.

1. Introduction

Observational data shows that Oxygen Deficient Zones (ODZs) have been expanding over the past several decades (Breitburg et al., 2018) in line with climate model outputs projecting a reduction in oceanic oxygen (O_2) in response to climate warming (Oschlies, 2021). The intensification and expansion of O_2 deficient areas of the ocean has been linked to a temperature driven increase in O_2 solubility in the surface ocean (Keeling et al., 2010) coupled with enhanced water column stratification leading to reduced O_2 redistribution at depth (Li et al., 2020). The Pacific Ocean is presently host to one of the most extensive areas of O_2 deficient waters with well-defined areas of minimum O_2 concentrations existing in subsurface waters (200 – 1000 m) both north and south of the equator along the eastern margin (Fig. 1B). Subsurface O_2 concentration is dependent on supply and consumption. Consumption of oceanic O_2 is modulated by the strength and efficiency of the biological carbon pump (BCP) determining both the amount of organic carbon produced via primary productivity and its subsequent transfer to the deep ocean. The eastern tropical Pacific (ETP) is highly productive, representing 10 % of global primary production (Pennington et al., 2006) influenced by the injection of nutrients via wind-driven shoaling of the thermocline (Helly and Levin, 2004). These regions of high primary productivity influence O_2 depleting conditions through the export and remineralization of sinking organic matter consuming O_2. Ocean circulation influences the supply and distribution of O_2 with limited ventilation and long water residence times contributing to reduced O_2 concentrations within Pacific deep and intermediate waters (Karstensen et al., 2008). Intrinsically linked to these biogeochemical and physical processes governing O_2 concentration and distribution within the Pacific Ocean is both the sequestration and release of CO_2; today the ETP represents a region of air-sea disequilibrium due to the flux of CO_2 to the atmosphere via upwelling of deep and intermediate waters (Takahashi et al., 2009). The ETP may have been an important carbon reservoir during the last glacial period (Jacobel et al., 2020) facilitated by the expansion of O_2 depleted waters (Hoogakker et al., 2018) in response to reduced ventilation (Skinner et al., 2015), a stronger BCP (Jaccard and Galbraith, 2012) or O_2 disequilibrium (Cliff et al., 2021). Following deglaciation, this pool of respired carbon is thought to have been an important CO_2 source via

* Corresponding authors.
E-mail addresses: katrina.nilsson-kerr@uib.no (K. Nilsson-Kerr), b.hoogakker@hw.ac.uk (B.A.A. Hoogakker).

https://doi.org/10.1016/j.epsl.2025.119253
Received 12 August 2024; Received in revised form 4 February 2025; Accepted 9 February 2025
Available online 14 February 2025
0012-821X/© 2025 The Author(s). Published by Elsevier B.V. This is an open access article under the CC BY license (http://creativecommons.org/licenses/by/4.0/).

increased ventilation of intermediate and deep waters (Anderson et al., 2009; Martínez-Botí et al., 2015; Ronge et al., 2021; Shuttleworth et al., 2021). Despite the important coupling between oceanic O_2 and carbon cycling, long-term reconstructions of oceanic O_2 are lacking. The Pacific Ocean is thought to have been distinctly different across the late Miocene and early Pliocene, characterised by altered meridional and zonal sea surface temperature gradients (Zhang et al., 2014; Herbert et al., 2016) with consequences for wind-driven upwelling (Dekens et al., 2007; Drury et al., 2018; Shankle et al., 2021), while gateway changes were occurring at the eastern and western margins (Karas et al., 2017). Amongst this backdrop of basin-wide departures from a contemporary Pacific, large-scale climatic changes were taking place. Namely, the progressive expansion of ice in the high latitudes of both hemispheres (Evangelinos et al., 2024; Leutert et al., 2020; Raymo, 1994) with attendant changes in global oceanic and atmospheric circulation patterns (Butzin et al., 2011; Groeneveld et al., 2017). Collectively, and individually, these factors would have exerted competing influences on Pacific Ocean O_2 concentrations and distribution, with consequences for CO_2.

The application of iodine to calcium ratios (I/Ca) in both planktic and benthic foraminifera is an emerging proxy for subsurface and bottom water O_2 concentrations, respectively (Glock et al., 2014; Hess et al., 2023; Hoogakker et al., 2018; Lu et al., 2016; W. Lu et al., 2020; Zhou et al., 2014) owing to iodine's redox sensitivity (Rue et al., 1997). The exploitation of foraminiferal shell geochemistry to determine I/Ca stems from the ability of the oxidized species of iodine, iodate (IO_3^-), to substitute with CO_3^{2-} in $CaCO_3$ (Feng and Redfern, 2018). The concentration of IO_3^- in seawater as it reduces to iodide (I^-) under O_2 reducing conditions is manifested as lower foraminiferal I/Ca. Due to the combined nature of iodine speciation and mixing effects in the water column, it has been inferred that the I/Ca of planktic foraminifera does not reflect *in-situ* conditions but influenced by vertical advective processes (Chance et al., 2014; Hardisty et al., 2021; W. Lu et al., 2020; Zhou et al., 2015). It has been proposed, based on core-top calibration studies, that I/Ca values of < 2.5 μmol/mol reflect dissolved O_2 concentrations in subsurface waters of < 70 μmol/mol, indicative of hypoxic conditions (Lu et al., 2016; W. Lu et al., 2020) whilst I/Ca values of > 4 μmol/mol are thought to indicate well-oxygenated subsurface waters with dissolved O_2 concentrations of > 100 μmol/mol (Lu et al., 2016; W. Lu et al., 2020). However, this relationship has been recently complicated by the results of a plankton tow study which found a limited distinction between I/Ca values with dissolved O_2 concentrations (Fig. 2A) (Winkelbauer et al., 2023). Additionally, the values obtained (< 1 μmol/mol) were an order of magnitude different to that of reported core-top values (Fig. 2A). This discrepancy was suggested to be due to an additional gain of IO_3^- post-mortem potentially biasing fossil foraminifera shell I/Ca signatures (Winkelbauer et al., 2023). Thus, complicating the application and interpretation of I/Ca in planktic foraminifera as a proxy for paleo-O_2 concentrations. Nonetheless, previous studies utilising I/Ca in planktic foraminifera have proven useful in gaining insights into paleo-O_2 conditions with results corroborated by additional lines of proxy evidence (Hess et al., 2023; Hoogakker et al., 2018).

To assess how the oxygenation state of the tropical Pacific responded to changes in both regional and global climate across the late Cenozoic (16 – 0 Ma) we apply I/Ca of planktic foraminifera from deep sea sediments as a proxy for redox conditions at ODP Sites 806 (0°19.1′N, 159°21.7′E, 2521 m), 1236 (21°21.538′S, 81°26.146′W, 1322 m), 1237 (16°01.421′S, 76°22.685′W, 3212 m) and IODP Site U1338 (2°30.469′N, 117°58.178′W, 4200 m). Subsurface waters above ODP Site 1237 are located within the Southeast Pacific ODZ whilst subsurface waters above ODP Site 1236 and IODP Site U1338 sit at the fringes of the Southeast and Northeast Pacific ODZ (Fig. 1A). To further enable interpretation of our downcore I/Ca records, we have expanded the I/Ca–O_2 calibration (Lu et al., 2016; W. Lu et al., 2020) by incorporating 89 datapoints from the Pacific and Indian Oceans (Fig. 2, S2). Our expanded calibration dataset includes material spanning a range of O_2 concentrations and bolsters sample representation of environments with subsurface O_2 levels < 100 μmol/mol (Fig. 2). We also make observations of the occurrence of planktic foraminifera species *Globorotaloides hexagonus*. In a recent study, Davis et al. (2023) propose that this subsurface dwelling planktic foraminifera species may be used to trace the extent and intensity of low O_2 subsurface waters and subsequently used this proxy to demonstrate the widespread existence of pelagic oxygen minimum zones during the Pliocene (Davis et al., 2023). Together with published planktic foraminifera bound nitrogen isotope records (FB-$\delta^{15}N$), our new results are used to assess the evolution of the Pacific ODZ over the past 16 Myr. We then evaluate the evolution of the eastern Pacific ODZ in the context of wider Pacific basin water mass and ventilation changes, using published neodymium isotope compositions (εNd) and benthic foraminifera carbon isotope records ($\delta^{13}C$).

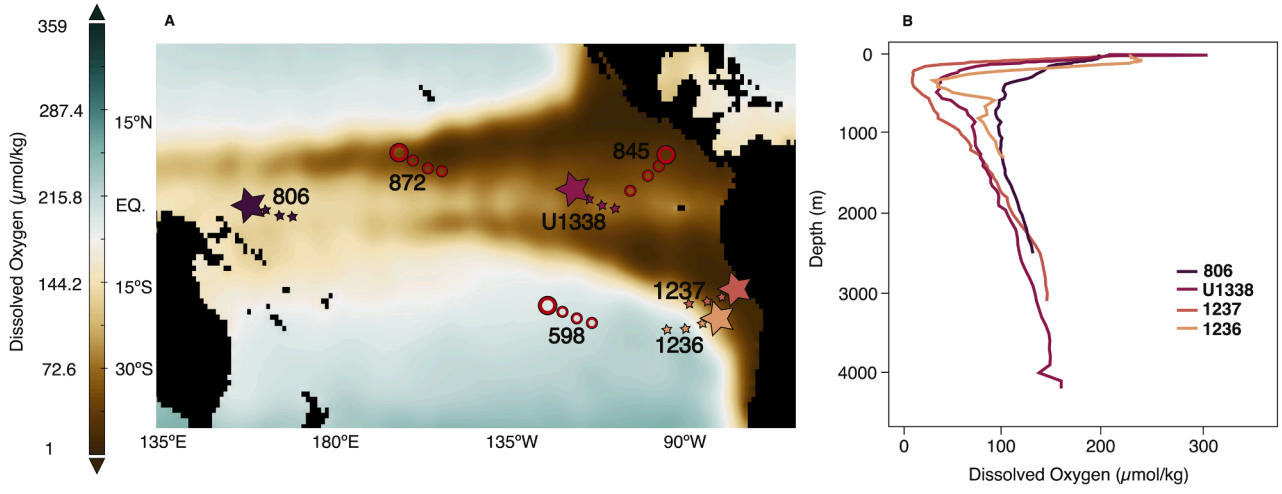

Fig. 1. Spatial characteristics of O_2 depleted waters in the tropical Pacific subsurface (A) O_2 concentrations from the WOA2018 dataset at 300 m water depth (1995 – 2010) (Garcia et al., 2019). Study locations shown with backtracked positions (small stars) illustrated in 5 Ma increments starting from 15 Ma through to the present-day site location (largest star) (Müller et al., 2018) with previously published study sites that track O_2 depletion and referred to in this study (i.e. DSDP Site 598 and ODP Sites 845 and 872) indicated by open red circles, similarly with the largest circle representing the present-day site location (Auderset et al., 2022; Hess et al., 2023; Wang et al., 2022) and (**B**) vertical profiles of dissolved O_2 (Garcia et al., 2019) at each of the present-day site locations of this study.

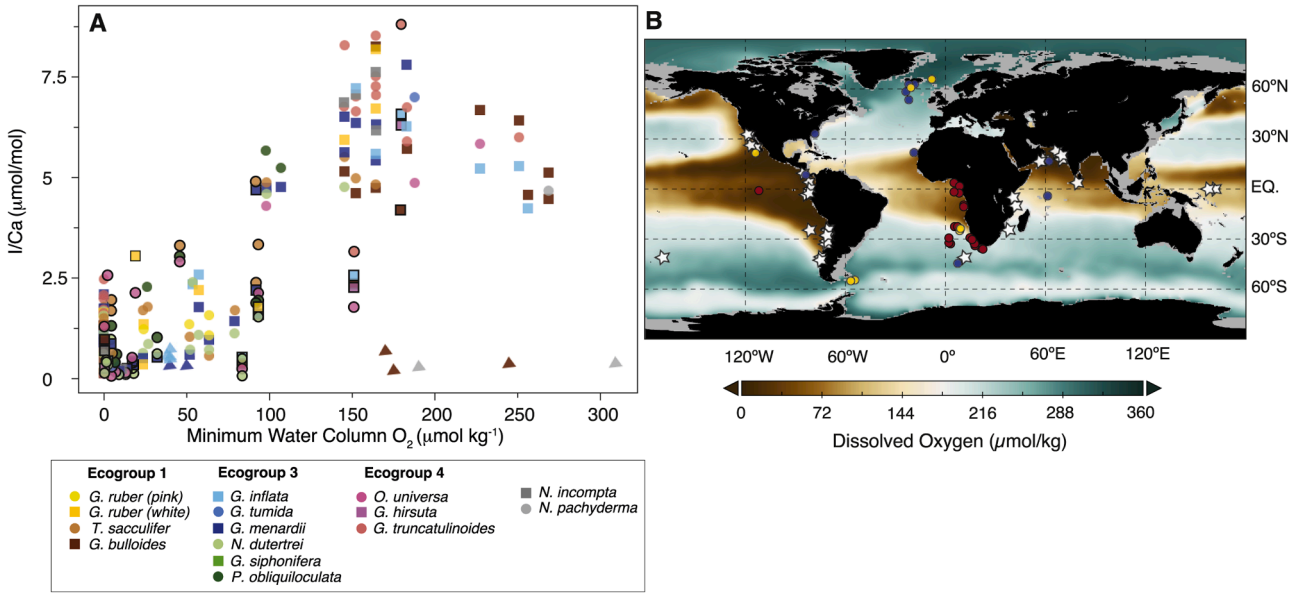

Fig. 2. Expanded I/Ca-O_2 Core-top Calibration (A) Published I/Ca ratios from planktic foraminifera core-top studies (filled circles, squares) (Lu et al., 2016; W. Lu et al., 2020), plankton tow study (Winkelbauer et al., 2023) (filled triangles) and new data from this study (circles, squares outlined in black) against minimum dissolved water column O_2 concentrations and (**B**) O_2 concentrations from the WOA2018 dataset at 300 m water depth (1955 – 2010) (Garcia et al., 2019) with white stars representing locations of new data from this study, yellow circles representing the location of plankton tow I/Ca (Winkelbauer et al., 2023), blue circles representing the core-top data from Lu et al. (2016) and red circles representing the core-top data from W. Lu et al. (2020).

2. Materials and methods

2.1. Core-top and down-core material

A total of 58 sediment samples from the Indian and Pacific Oceans were provided by the Lamont-Doherty Core Repository, 4 samples from the Ocean Discovery Program (ODP) and 8 samples from the GeoB Bremen-MARUM core repository (Table S2).

Down-core material was sourced from 4 sites straddling the equatorial Pacific with ODP Site 806 and 1236 positioned on the fringes of the modern-day ODZ and IODP U1338 and ODP 1237 situated within the core ODZ to assess changes in ODZ extent and intensity over time (Fig. 1A). ODP 806 (0°19.1′N, 159°21.7′E), located atop the Ontong Java Plateau in the western equatorial Pacific, was drilled at a water depth of 2521 m during Leg 130 (Kroenke et al., 1991). ODP Sites 1237 (16°01.421′S, 76°22.685′W) and 1236 (21°21.538′S, 81°26.146′W), both located atop the Nazca Ridge off the Peruvian coast were drilled during Leg 202 at water depths of 3212 and 1322 m respectively (Mix et al., 2003). IODP Expedition 320/321 Site U1338 (2°30.469′N, 117°58.178′W) was drilled at a water depth of 4200 m (Pälike et al., 2010).

Today the deep Pacific Ocean is bathed by a water mass comprising of southern-sourced deep waters, a mixture of Antarctic Bottom Water and North Atlantic Deep Water (NADW), which is exported from the Antarctic Circumpolar Current into the Southwest Pacific and advected northwards prior to returning south along the eastern Pacific (Talley et al., 2011). This Pacific Deep Water (PDW) characterizes the deep waters bathing IODP Site U1338 and ODP Sites 1237 and 806. The shallowest site, ODP 1236, is located within the mixing zone between this O_2 depleted and nutrient enriched PDW with better oxygenated Antarctic Intermediate Water (Talley et al., 2011). The subsurface circulation of all sites is influenced by the eastward flowing Equatorial Undercurrent, a mixture of Antarctic Intermediate Water and Sub-Antarctic Mode Water (Kessler, 2006). Whilst intermediate waters in the ETP are influenced by a geochemically distinct Equatorial Pacific Intermediate Water, a combination of Antarctic Intermediate Water and PDW (Bostock et al., 2010). These intermediate waters are thought to exert a prominent role in determining the spatial characteristics of the ODZs in the eastern equatorial Pacific (EEP) (Busecke et al., 2019) through the contribution of cold, nutrient enriched waters which are upwelled to the surface (Tsuchiya et al., 1989) supporting primary productivity (Pennington et al., 2006).

2.2. Age model

We utilise the updated age model for ODP Sites 806 and 1236 presented in Li et al. (2023); initially reported magnetochron and microfossil biochronology has been transferred onto the Geological Timescale 2012 (GTS2012) (Gradstein and Ogg, 2012). We follow this approach for ODP Site 1237; converting reported magnetochron and microfossil biochronology (Kroenke et al., 1991) to the GTS2012 timescale (Gradstein and Ogg, 2012). We additionally refine the age model presented in Holbourn et al. (2022) based on high-resolution benthic isotope stratigraphy. For IODP Site U1338, the age model across the mid-Miocene (12 – 16 Ma) follows Holbourn et al. (2022) and across the late Miocene-Pleistocene (0 – 8 Ma) follows Lyle et al. (2019) with linear interpolation applied between 8 – 12 Ma.

2.3. I/Ca analysis

Preparation of planktic foraminifera specimens for I/Ca analysis follows the methods outlined in Winkelbauer et al. (2021). For core-top I/Ca analysis, a selection of 20 – 70 planktic foraminifera specimens inhabiting surface and thermocline waters were picked from the > 300 µm size-fraction. Whilst for the long-term downcore records > 40 individuals were picked from the > 250 µm size-fraction. Samples were treated monospecifically. Specimens were crushed between two glass slides prior to undergoing the clay removal step following Barker et al. (2003). Samples subsequently underwent an extended oxidative cleaning step to ensure the adequate removal of organic material that may bias I/Ca values (Winkelbauer et al., 2021). This consisted of each sample undergoing a minimum of three rinses in buffered 1 % (v/v) H_2O_2 at boiling point for ten minutes with brief ultrasonification at 5 mins and agitation at 2.5 and 7.5 mins. Following the oxidative step, samples were polished with a dilute (0.001 M) HNO_3 leach. Analysis follows the procedures outlined in Winkelbauer et al. (2021). Samples

were dissolved in ultrapure (0.5 – 3 %) HNO_3 on the day of analysis, centrifuged and split into two vials for I/Ca and trace element analysis. Aliquots for I/Ca analyses were stabilized with Tetramethylammonium hydroxide (TMAH) to attain a basic pH (> 7). I/Ca and trace element ratios were measured using an Agilent Technologies 8900 ICP-MS instrument at the Inorganic Geochemistry Facilities, BGS. The long-term precision based on repeat measurements of JCP-1 as an internal monitoring standard for I/Ca is 0.6 μmol/mol.

3. Results

A total of 89 I/Ca measurements from modern/Holocene sediment core-tops, consisting of 12 different planktic foraminifera species were analysed to expand the I/Ca–O_2 calibration (Lu et al., 2016; W. Lu et al., 2020). Samples were confirmed to be modern/Holocene in age through radiocarbon dating and benthic foraminifera oxygen isotope ($\delta^{18}O$) assessments (Supplementary Text, Fig. S1). Measured I/Ca values range from 0.1 – 8.8 μmol/mol covering a range of minimum water column O_2 values of 0 – 200 μmol/kg. Specific geographic distinctions exist; low I/Ca values are found in the northern Indian Ocean (< 1 μmol/mol) and eastern Pacific (< 0.5 μmol/mol) whilst intermediate-to-high I/Ca values characterise the equatorial Indian Ocean (1 – 7 μmol/mol) and western Pacific (2 – 5 μmol/mol) (Fig. 2, S2). The eastern Pacific is characterised by the lowest reconstructed (<0.5 μmol/mol) I/Ca out of all regions (i.e. Indian Ocean, West Pacific and Atlantic Ocean) with available core-top data (Fig. S2) corresponding to minimum water column O_2 values ranging up to 100 μmol/kg (Fig. S2). Generally, lowest core-top I/Ca (< 1 μmol/mol) are confined to minimum water column O_2 concentrations of < 50 μmol/kg. A similar relationship is found between core-top I/Ca values with bottom water O_2 concentrations (Fig. S3). Generally, lower I/Ca values (< 0.5 μmol/mol) are confined to bottom water O_2 values of up to 150 μmol/kg (Fig. S3) whilst highest I/Ca values (> 5 μmol/mol) are associated with higher bottom water O_2 concentrations of > 150 μmol/kg (Fig. S3). Lowest bottom waters and I/Ca values are confined to locations from the eastern Pacific (Fig. S2B ii, S3). No discernible distinctions exist in I/Ca values associated with planktic foraminifera depth habitats with both mixed-layer and thermocline dwelling species exhibiting a range of I/Ca values across O_2 conditions. Out of the 31 core-tops measured in this study all except 3 had more than one species of planktic foraminifera analysed with no observed biases associated with inferred depth habitat (Fig. S2B, Table S2).

Long-term downcore I/Ca records were generated similarly by using a selection of planktic foraminifera species, a combination of both inferred mixed-layer and thermocline dwelling species, across the four selected sites (Fig. S4, Data S1). The selection of analysed planktic foraminifera, inferred to be inhabiting different depths within the water column based on the ecogrouping of Aze et al. (2011), show a limited distinction in I/Ca values corresponding to depth habitat (Fig. S4). Across all four down-core locations the highest I/Ca values (> 1 μmol/mol) are found during the middle Miocene (> 12 Ma). ODP Sites 1237 and 1236 record the highest I/Ca values of up to 7 μmol/mol whilst IODP U1338 and ODP 806 record values of up to 2 μmol/mol. It is noted that the planktic foraminifera I/Ca record of Hess et al. (2023) from ODP Site 845 (Fig. 1A) also shows high values during the middle Miocene with I/Ca values of up to 8 μmol/mol (Fig. 3A). The lowest reconstructed I/Ca (< 0.5 μmol/mol) values characterise IODP Site U1338 with low I/Ca values characterising the late Miocene and Pliocene (~9 – 2 Ma). A progressive reduction of I/Ca values at ODP Site 806 is similarly found from the late Miocene (< 10 Ma) onwards with lowest values (< 0.5 μmol/mol) attained by the Pliocene (~5 Ma). ODP Site 1237 similarly displays a progressive reduction in I/Ca values from the late Miocene onwards (< 10 Ma). ODP Site 1236 meanwhile records variable and higher I/Ca values throughout the reconstructed interval (Fig. S4). Low O_2 indicator species, G. *hexagonus* (Fig. S5), is first observed at ~7 Ma at IODP Site U1338 (Pälike et al., 2010) and ~7.75 Ma at ODP Site 1237 (Fig. 3A).

4. Discussion

4.1. Planktic foraminiferal I/Ca

The expanded I/Ca–O_2 calibration dataset presented in this study builds on previous efforts to refine the I/Ca–O_2 proxy based on core-top data (Lu et al., 2016; W. Lu et al., 2020). The increased spatial coverage of I/Ca core-top datapoints, especially in the Pacific and Indian Ocean ODZs, provides further support for the correspondence between low planktic foraminifera I/Ca values in regions characterised by low subsurface O_2 concentrations.

The relationship between O_2 and I/Ca, however, is not linear (Fig. 2A). This is consistent with documented O_2–IO_3^- water column profiles and iodine speciation studies, highlighting the complexities of redox reactions in determining the reduction of IO_3^- (Hardisty et al., 2021; Farrenkopf and Luther, 2002; Moriyasu et al., 2020).

The core-top data presented in this study corroborates the existence of a discrepancy between core-top data and reported plankton tow I/Ca values (Fig. 2A). Foraminiferal $CaCO_3$ has been shown to be susceptible to recrystallization during export through the water column and subsequent deposition and burial at depth (Davis and Benitez-Nelson, 2020) with the greatest susceptibility of $CaCO_3$ to recrystallization occurring imminently post-mortem (Chanda et al., 2019). This scenario of planktic foraminifera I/Ca being predominantly affected by post-mortem processes has been disputed by Lu et al. (2023) following reconstruction of low planktic foraminifera I/Ca values in ODZ regions underlain by high O_2 bottom waters, in combination with benthic foraminifera derived data for comparison (Lu et al., 2023). However, very low I/Ca values may reflect foraminifera shell dissolution and reprecipitation of secondary calcite occurring in the presence of I^- saturated pore and bottom waters (Branson et al., 2015; Hardisty et al., 2017; Lau and Hardisty, 2022). Increased concentrations of I^- has been observed in porewaters associated with both reducing conditions and influence from degrading organic matter (Anschutz et al., 2000). Whilst other studies suggest a lack of correlation between expected I^- concentrations and bottom water O_2 content when compared to observed concentrations in ODZ regions (Evans et al., 2024). Instead, recent work suggests predicting I^- concentrations is not only attributed to regions of low O_2, but also where water column/porewaters are high in sulphide concentrations (Evans et al., 2024). Taken together, a simple attribution of iodine reducing conditions remains complex with regional processes exerting a strong control on both the speciation of iodine and concentrations of I^-.

We infer the very low I/Ca values obtained at our study sites (< 1 μmol/mol) from the late Miocene through the Pleistocene (Fig. 3A) as reflecting a limited influence of secondary IO_3^- incorporation in the presence of high O_2 concentrations. However, we cannot distinguish between I/Ca incorporation due to the presence and advection of bottom/porewater reducing conditions in governing the reconstructed I/Ca signatures. To assess preservation, we undertook Scanning Electron Microscopy (SEM) to further constrain the potential authenticity of I/Ca values. SEM images display foraminifera to be generally moderately-to-poorly preserved with a frosty textural appearance and evidence of recrystallization (Fig. S6). Specimens selected for SEM analysis across samples from IODP Site U1338 and ODP 1236 are consistently moderate-to-poorly preserved whilst samples from ODP Sites 1237 and 806 show poorer preservation prevalent in older samples (Fig. S6). At ODP Site 806 we find very low planktic foraminifera I/Ca ratios, like ODP Site 1237, across the past 10 Myr which is at odds given the location of ODP Site 1237 within the modern-day core of the ODZ and ODP 806 being situated at the periphery. Thus, the very low values obtained at these sites may be influenced by secondary diagenetic processes biasing a primary I/Ca signature. The shallowest of the sites, ODP Site 1236 (1322 m), records both high and variable I/Ca values suggesting the potential influence of secondary IO_3^- incorporation in the

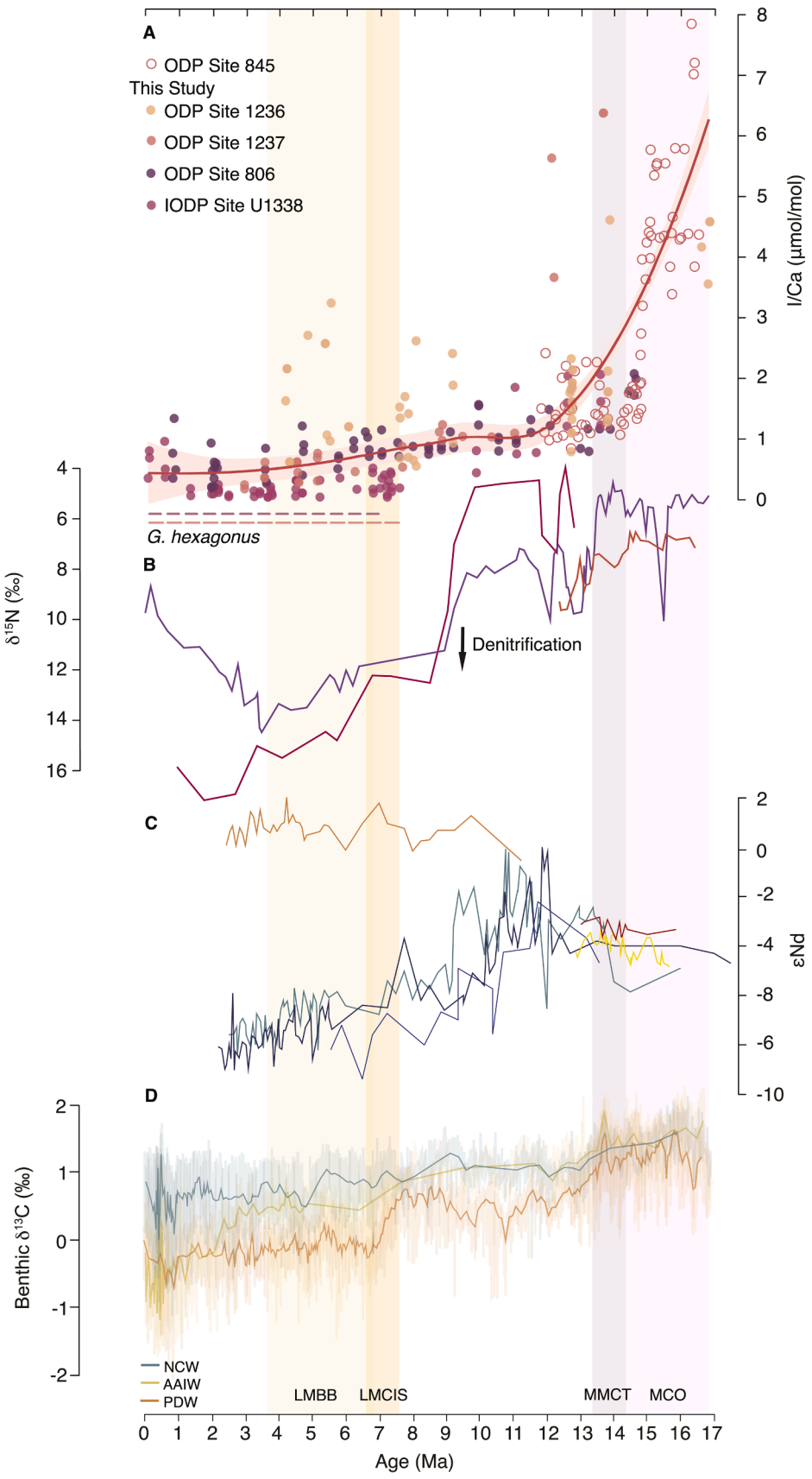

(caption on next page)

Fig. 3. Late Cenozoic deoxygenation of the Pacific Ocean A) Planktic foraminifera I/Ca records, filled circles are data from this study and open circles are from ODP Site 845 (Hess et al., 2023) with a LOESS fit and 95 % confidence interval (pink line), dashed lines indicate presence of G. hexagonus at ODP Site 1237 and IODP U1338 (Pälike et al., 2010) **B**) Foraminifera bound $\delta^{15}N$ records from across the tropical Pacific Ocean; ODP Site 845 (red line) (Hess et al., 2023), ODP 872 (deep pink line) (Wang et al., 2022) and DSDP 598 (purple line) (Auderset et al., 2022) **C**) εNd records from the Pacific; ODP 1236 (yellow line) (Holbourn et al., 2013), ODP Site 1237 (red line) (Holbourn et al., 2013) and ODP 1241 (orange line) (Osborne et al., 2014) and from the Caribbean; ODP Site 999 (turquoise line) (Newkirk and Martin, 2009), ODP 998 (dark blue line) (Newkirk and Martin, 2009) and ODP 1006 (blue line) (Kirillova et al., 2019) and **D**) Compiled benthic foraminiferal $\delta^{13}C$ records grouped by depth representing inferred circulation end-members (see Table S1 for reference information); Northern Component Water (NCW) (blue line), Antarctic Intermediate Water (AAIW) (yellow line) and Pacific Deep Water (PDW) (orange line) with 250-pt running mean average in bold. Shaded bars represent key periods of the Miocene; Miocene Climatic Optimum (MCO), Middle Miocene Climate Transition (MMCT), Late Miocene Carbon Isotope Shift (LMCIS) and the Late Miocene Biogenic Bloom (LMBB).

presence of better oxygenated bottom waters. Thus, the I/Ca proxy is currently limited to providing an empirical inference on O_2 levels with further work required on marine iodine cycling and susceptibility of I/Ca in foraminifera to diagenetic alteration to allow for more detailed constraints.

4.2. Development of the eastern Pacific ODZ

Due to the caveats discussed in Section 4.1, we cautiously interpret our downcore planktic foraminifera I/Ca records as being representative of an integrated water column/porewater signal rather than solely subsurface O_2 conditions.

Importantly, we find the sustained presence of *Globorotaloides hexagonus* in samples from ODP Site 1237 from the late Miocene (7.75 Ma) like that in timing of the reported presence of this species at IODP Site U1338 (~7 Ma, Fig. 3A), whilst at ODP Site 1236 they have a reported uncommon occurrence (Pälike et al., 2010). This is a deep-dwelling planktic foraminifera species inferred to prosper in subsurface waters severely depleted in O_2 (Davis et al., 2023). The correspondence between the coeval presence of this species and low I/Ca values at ODP Site 1237 and IODP Site U1338 by ~8 – 7 Ma (Fig. 3A) also indicates that the signal at ODP Site 1237 is likely not dictated by plate movements of the site eastwards across the mid-late Miocene (Fig. 1A). Thus, the appearance of G. *hexagonus* from 8 – 7 Ma, in conjunction with low planktic foraminifera I/Ca values, hints at the onset of severely O_2 depleted subsurface waters characterising the eastern Pacific which we attribute to the emergence of the ODZ.

Supporting evidence for the emergence of severely depleted subsurface waters in this region also comes from planktic foraminifera bound nitrogen isotopes (FB-$\delta^{15}N$). Records from across the tropical Pacific show relatively low FB-$\delta^{15}N$ during the middle Miocene (Fig. 3B), likely indicative of well oxygenated subsurface waters characterized by limited water column denitrification (Auderset et al., 2022; Hess et al., 2023; Wang et al., 2022). Hess et al. (2023) pose that the spatial extent of denitrification in the ODZ became more comparable today around 13.6 Ma. However, the studies of Auderset et al. (2022) and Wang et al. (2022) indicate an intensification of denitrification due to a greater increase in FB-$\delta^{15}N$ after ~10

Ma (Fig. 3B). DSDP Site 598 in the South Pacific shows an almost 8 ‰ increase between 10 and 8.5 Ma (Wang et al., 2022), whereas that of ODP Site 872 from the North Pacific (Auderset et al., 2022) shows a more modest increase of 3.5 ‰. The FB-$\delta^{15}N$ values between these two sites are consistent with each other between 8.5 and 3.5 Myr, continuing with an increasing trend in FB-$\delta^{15}N$. Subsequently, the South Pacific FB-$\delta^{15}N$ values stabilize whilst the North Pacific ODP Site 872 FB-$\delta^{15}N$ values continue to decrease (Fig. 3B). The significant increase in FB-$\delta^{15}N$ between 10 and 3.5 Ma has been interpreted as having been driven by an intensification of subsurface water denitrification under deteriorating O_2 conditions (Auderset et al., 2022; Wang et al., 2022). The appearance of G. *hexagonus* at ODP Site 1237 and IODP Site U1338 occurs just after the increase in FB-$\delta^{15}N$ at DSDP Site 598 and ODP Site 872, supporting the notion of deteriorated subsurface O_2 concentrations and representing the manifestation of ODZ waters in the region around 8 – 7 Ma. We note that there is a discernible discrepancy in timing between the appearance of G. *hexagonus* and increase in FB-$\delta^{15}N$ versus the lowering of planktic foraminifera I/Ca values, which occurs much earlier between 14 – 11 Ma (Fig. 3A, B). This discrepancy in timing between the different proxies could either be explained by 1) bottom water processes, where high bottom water O_2 concentrations may have caused planktic foraminifera to gain additional IO_3^- post-mortem or 2) attributed to the higher threshold of iodine reduction in the water column associated with O_2 content compared with denitrification (Rue et al., 1997). The reduction of iodine occurs prior to denitrification (Cutter et al., 2018) and thus, this discrepancy in timing between I/Ca with FB-$\delta^{15}N$ may act as an indication on the spatial and temporal progression of ODZ development across the mid-late Miocene.

4.3. Ocean circulation changes and Pacific Ocean O_2

A crucial regional facet of the Pacific across the Miocene-Pliocene is the progressive Closure of the Central American Seaway (CAS) and emergence of the Panama Isthmus. Absolute temporal constraints on both CAS closure and presence of a fully emerged Panama Isthmus remains fragmentary (Jaramillo et al., 2017; O'Dea et al., 2016). However, it is generally thought that there was a cessation of a deep-to-intermediate water connection between the Pacific and Atlantic by the mid-late Miocene (Kirillova et al., 2019; Newkirk and Martin, 2009), whilst surface exchange persisted via shallow water straits until the Pliocene (Steph et al., 2006). The closure of the CAS and successive termination of shallow water exchange is thought to have exerted a critical role in the evolution of late Cenozoic cooling, with both modelling (Nisancioglu et al., 2003; Zhang et al., 2011) and proxy studies (Auderset et al., 2019; Osborne et al., 2014) converging to highlight the strengthening of deep-water formation in the North Atlantic with a closed CAS. The radiogenic Nd isotope composition (εNd) of fossil fish teeth and planktic foraminifera coatings, interpreted as water mass tracers, suggest deep water exchange was impeded by ~11 Ma and that a progressive trend in Caribbean εNd towards less radiogenic values across the late Miocene-Pliocene (Fig. 3C) reflects a gradual reduction in the contribution of Pacific waters to the Atlantic, combined with Atlantic Meridional Overturning Circulation strengthening (Newkirk and Martin, 2009; Osborne et al., 2014). Recent modelling work (Khon et al., 2023) further suggests that in the absence of a closed CAS and presence of a shallow sill, enhanced transport of O_2-enriched subsurface waters from the Pacific to the Atlantic may have influenced the ETP to be bathed in better ventilated subsurface waters, whilst a deep sill would have permitted better ventilation of the deep interior Pacific through inflowing NADW. An initial depletion in Pacific Ocean benthic foraminifera $\delta^{13}C$ during the Miocene (Fig. 3D) (< 13 Ma) has been inferred as an invigoration of the meridional overturning circulation (Holbourn et al., 2022; Lear et al., 2003). This invigoration of ocean circulation is suggested to be driven by a cessation of Atlantic-Pacific deep-water exchange (Khon et al., 2023), as evidenced by diverging εNd in the Pacific across this period (Fig. 3C) and a depletion in benthic foraminifera $\delta^{13}C$ from deep Pacific Ocean sites (Fig. 3D).

A second stepwise decrease in benthic foraminifera $\delta^{13}C$ values inferred to represent PDW (Fig. 3D) coincides with the appearance of G. *hexagonus* and evidence for intensified denitrification in the ETP (Fig. 3B). We interpret the decrease in $\delta^{13}C$ around 8 Ma as the

culmination of ocean circulation and ventilation changes in relation to a more or less complete closure of the CAS. Modelling work shows that the volume of low O_2 waters in the EEP significantly increase when the CAS shoals from ~200 m (Khon et al., 2023). If the expansion of low O_2 waters in this region were accompanied by an intensification of the ODZ, then the increasing FB-$\delta^{15}N$ values from 10 Ma (Fig. 3B) could potentially reflect a progressive shoaling of the CAS. We infer that Atlantic-Pacific surface water exchange persisted through relatively shallow (< 100 m) straits between 8.5 – 3.5 Ma but that this shallow exchange ceased around 3.5 Ma. Thus, in combination with our results, we infer that the mid-late Miocene termination of deep-water exchange between the Atlantic and Pacific, and corresponding onset of a circulation pattern akin to modern, played a pivotal role in determining the oxygenation state of the tropical Pacific.

4.4. *The biological carbon pump, O_2 and carbon cycling*

The late Cenozoic is associated with a progressive decline in atmospheric CO_2 (Fig. 4E) which is inferred to have played a decisive role in the accompanying global cooling from the middle Miocene through to Pleistocene (Brown et al., 2022). Higher Pacific O_2 concentrations (16 – 13 Ma) coincide with a period of elevated atmospheric CO_2 concentrations (Fig. 4E) and reduced organic carbon burial (Fig. 4D). This reduction in organic carbon burial has been attributed to a temperature driven weakening and/or reduced efficiency of the BCP (Li et al., 2023). The temperature dependence of bacterial respiration has been inferred to have promoted both faster and shallower remineralization of particulate organic carbon during the climatic warmth of the middle Miocene thereby resulting in reduced organic carbon burial (Boscolo-Galazzo et al., 2021). This is in line with productivity records based on $CaCO_3$ and opal mass accumulation rates at IODP Site U1338 (Fig. 4D) which suggests that the middle Miocene experienced much higher rates of primary productivity compared to the late Pleistocene, facilitated by enhanced nutrient availability via remineralizing particulate organic carbon (Lyle and Baldauf, 2015). This weakened efficiency of the BCP during the middle Miocene may have exerted a critical role in contributing to the elevated atmospheric CO_2 levels (Fig. 4E). However, faster rates and corresponding shallower remineralization of organic matter during this period was inferred to have contributed to an upward extension of the ODZ in response to increased subsurface respiration (Li et al., 2023). This upward expansion of the ODZ was inferred to be a primary factor influencing a contracted niche, limited mainly to the mixed layer, of planktic foraminifera (Boscolo-Galazzo et al., 2021; Woodhouse et al., 2023). However, this inferred expansion of the ODZ during the middle Miocene is at odds with the suite of O_2 proxy records (I/Ca, absence of G. *hexagonus* and FB-$\delta^{15}N$) suggesting better oxygenated conditions (Fig. 3(4) A, B). We infer the contribution of better ventilated deep and intermediate waters to have counteracted any diminishment of Pacific Ocean O_2 in response to high primary productivity and bacterial respiration promoting shallower remineralization of particulate organic carbon.

The onset of sustained low O_2 conditions (8 – 7 Ma) accompanies perturbations in the carbon cycle across the late Miocene. A change in the efficiency and strength of the BCP occurs during the Late Miocene Biogenic Bloom (Fig. 4D) following the establishment of modern-like benthic foraminifera $\delta^{13}C$ inter-basin gradients (Fig. 3D) across the Late Miocene Carbon Isotope Shift (~7 Ma). A globally coherent reorganization of atmospheric circulation is thought to have occurred during this period with ocean temperature records indicating a strengthening of the Pacific zonal temperature gradient and meridional temperature gradients (Fig. 4C) concordant with evidence of Northern Hemisphere onset of glaciation (Raymo, 1994). Taken together, this change in atmospheric circulation is thought to have promoted the Late Miocene Biogenic Bloom via attendant feedbacks such as enhanced nutrient input to the oceans (Holbourn et al., 2022) or increased upwelling of nutrient-rich deep and intermediate waters (Lear et al., 2003). Both of which would have exerted an influence on the BCP with increased O_2 consumption rates in subsurface waters and burial of organic material contributing to reducing pore-water conditions at depth. The paucity of pCO_2 records (Fig. 4E) across the Miocene-Pliocene renders it difficult to directly establish the influence these changes in Pacific Ocean biogeochemical cycling exerted on ocean carbon storage and sequestration of CO_2. However, the sustained decline in pCO_2 from the middle Miocene through the late Miocene-Pliocene accompanying decreased oceanic O_2 content would suggest a role for the tropical Pacific in carbon sequestration across the late Cenozoic, akin to that reconstructed for glacial periods (Anderson et al., 2009; Cliff et al., 2021; Hoogakker et al., 2018; Jaccard et al., 2012; Jacobel et al., 2020; Skinner et al., 2015).

5. Conclusions

In this study, we have provided additional constraints on the correspondence between low planktic foraminifera I/Ca in regions of low subsurface O_2 by expanding the I/Ca–O_2 core-top calibration dataset. However, attributing threshold O_2 levels to specific I/Ca values remains difficult considering the complexities in iodine speciation, regional variations in advective processes and biological productivity influencing iodine reduction rates (Cutter et al., 2018; Evans et al., 2024; Hardisty et al., 2021). The fidelity of the I/Ca proxy in its ability to reconstruct subsurface O_2 concentrations in the geological past thereby necessitates multi-proxy approaches to accurately make inferences on O_2 conditions. Nonetheless, invaluable insights on paleo-O_2 conditions can still be gained. The combination of our I/Ca results with the presence/absence of G. *hexagonus* and published FB-$\delta^{15}N$ records (Auderset et al., 2022; Hess et al., 2023; Wang et al., 2022) suggests a decline in tropical Pacific O_2 across the late Miocene-Pliocene, starting from ~11 Ma, which we attribute to a combination of ventilation changes mediated by tectonic configuration and influence of the BCP. We infer the widespread prevalence of a modern-like ODZ in the ETP by 8 – 7 Ma. Our data, along with other lines of evidence, contributes to constructing an evolving picture of the oxygenation state of the Pacific Ocean across the late Cenozoic. The evolution of widespread O_2 deficient waters across the eastern and tropical Pacific during the late Cenozoic will likely have played a role in the facilitation of carbon sequestration, akin to mechanisms inferred at the glacial-interglacial timescale (Hoogakker et al., 2018; Jacobel et al., 2020).

Funding sources

UKRI Future Leaders Grant MR/S0342931/1 (B. A. A. H).

Data availability

All data needed to evaluate the conclusions in the paper are present in the Supplementary Materials. Data will also be publicly available at Pangaea.de.

CRediT authorship contribution statement

Katrina Nilsson-Kerr: Writing – review & editing, Writing – original draft, Visualization, Methodology, Investigation, Formal analysis, Data curation. **Babette A.A. Hoogakker:** Writing – review & editing, Writing – original draft, Validation, Supervision, Resources, Project administration, Methodology, Investigation, Funding acquisition, Formal analysis, Data curation, Conceptualization. **Dharma A. Reyes Macaya:** Writing – review & editing, Visualization, Methodology, Investigation, Formal analysis. **Helge A. Winkelbauer:** Writing – review & editing, Methodology, Investigation, Formal analysis, Data curation. **Elliott Hamilton:** Writing – review & editing, Methodology, Formal analysis. **Simon Chenery:** Writing – review & editing, Methodology, Formal analysis. **Catherine V Davis:** Writing – review & editing, Validation, Methodology. **Melanie J. Leng:** Writing – review & editing, Validation,

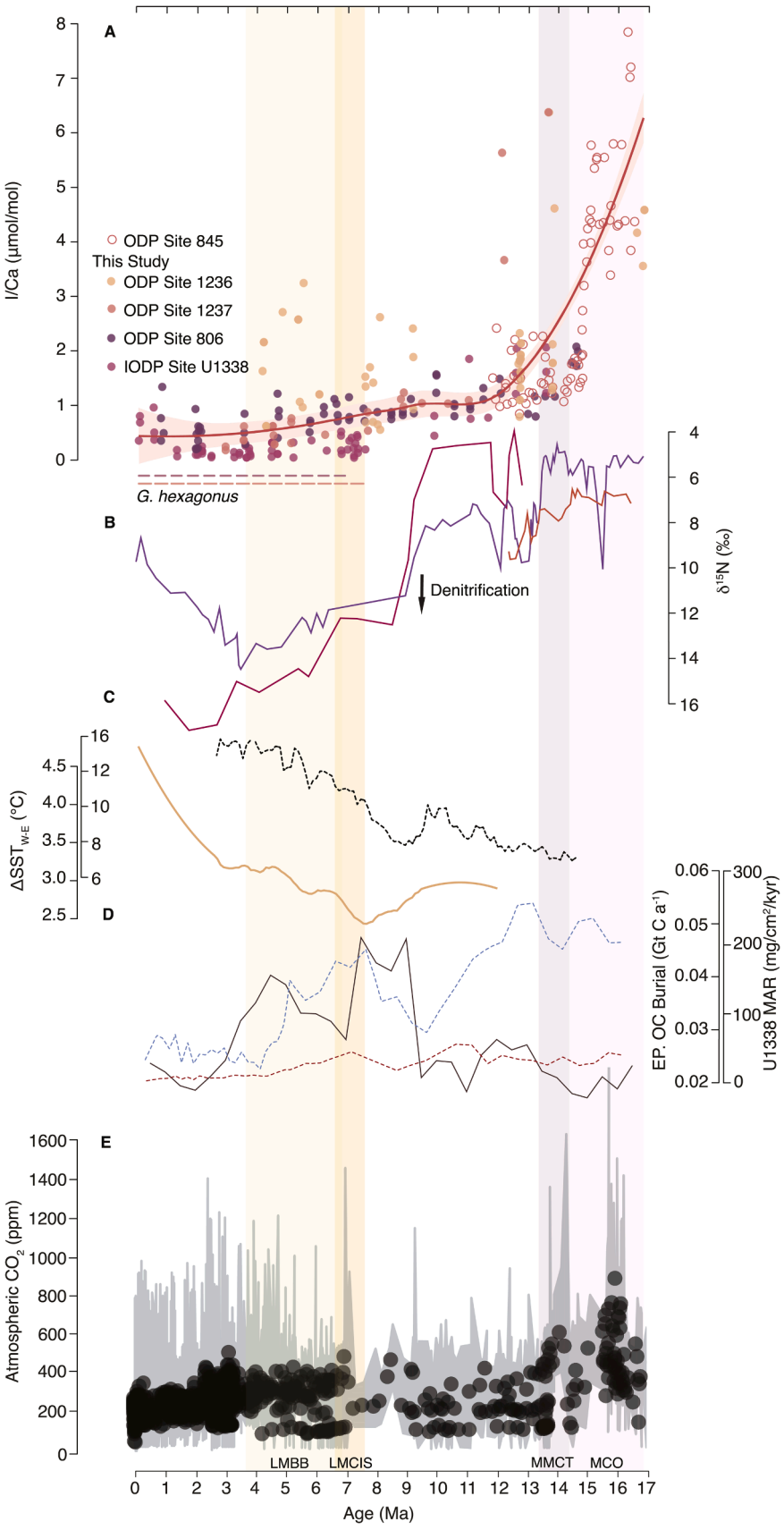

(caption on next page)

Fig. 4. Pacific Ocean deoxygenation and carbon cycling A) Planktic foraminifera I/Ca records, filled circles are data from this study and open circles are from ODP Site 845 (Hess et al., 2023) with a LOESS fit and 95 % confidence interval (pink line), dashed lines indicate presence of G. hexagonus at ODP Site 1237 and IODP U1338 (Pälike et al., 2010) **B**) Foraminifera bound $\delta^{15}N$ records from across the tropical Pacific Ocean; ODP Site 845 (red line) (Hess et al., 2023), ODP 872 (deep pink line) (Wang et al., 2022) and DSDP 598 (purple line) (Auderset et al., 2022) **C**) Pacific Zonal (W-E) SST gradient (orange line) (Zhang et al., 2014) and Northern Hemisphere (> 50°) SST anomaly (blue dashed line) (Herbert et al., 2016) **D**) Equatorial Pacific compilation of organic carbon mass accumulation rates (Li et al., 2023) (black solid line) and primary productivity based $CaCO_3$ (blue dashed line) and opal records (red dashed line) from IODP Site U1338 (Lyle and Baldauf, 2015) and **E**) Atmospheric CO_2 compilation (CenCO2PIP, 2023). Shaded bars represent key periods of the Miocene; Miocene Climatic Optimum (MCO), Middle Miocene Climate Transition (MMCT), Late Miocene Carbon Isotope Shift (LMCIS) and the Late Miocene Biogenic Bloom (LMBB).

Methodology.

Declaration of competing interest

The authors declare that they have no known competing financial interests or personal relationships that could have appeared to influence the work reported in this paper.

Acknowledgements

We acknowledge the effort from the crews and scientific parties of each of the respective cruises which retrieved the sediment samples necessary to undertake this study. This research used samples and/or data provided by the (Integrated) Ocean Drilling Program ((I)OPD). (I) ODP is/was sponsered by the US National Science Foundation and participating countires (NERC in the UK) under the management of Joint Oceanographic Institutions (JOI), Inc. Furthermore, this project used sample material provided by the Lamont-Doherty Core Repository of Lamont-Doherty Earth Observatory. We thank Dierk Hebbeln, Mayhar Mohtadi, Margarita Marchant and Robert F. Anderson for providing samples that were used in this study to expand the I/Ca–O2 calibration using core-top materials. We acknowledge the help provided by current researchers and former students from AG MARUM Marine Sedimentology and AF UdeC Micropaleontology (S. Figueroa, S. Giglio, M. Ramirez, M. Vergara, G.

Martinez-Mendez, A-L. Rugen, C. Soares) for their help in preparation of R/V S0156 core-top material. We thank Jim Buckman and Alba Navarro Rodriguez for assistance with SEM analysis. We acknowledge the contributions of Hilary Sloane and Kotryna Savickaite with stable isotope analysis at BGS and Phil Holdship with ICP-MS analysis at the University of Oxford. We acknowledge discussions surrounding the opening of the Panama Seaway with Raúl Trejos Tamayo. We acknowledge the invaluable contributions and comments from R. F. Anderson on a draft of this manuscript. Finally, we acknowledge the comments and suggestions of 2 anonymous reviewers and editor T. J. Horner in shaping this manuscript.

Supplementary materials

Supplementary material associated with this article can be found, in the online version, at doi:10.1016/j.epsl.2025.119253.

Appendix. Supplementary materials

Text.
Figs. S1-S8.
Tables. S1-S2.
Data. S1.

References

Anderson, R.F., Ali, S., Bradtmiller, L.I., Nielsen, S.H.H., Fleisher, M.Q., Anderson, B.E., Burckle, L.H., 2009. Wind-driven upwelling in the Southern Ocean and the deglacial rise in atmospheric CO2. Science (1979) 344, 84–87. https://doi.org/10.1126/science.1167441.

Anschutz, P., Sundby, B., Lefrançois, L., Luther III, G.W., Mucci, A., 2000. Interactions between metal oxides and species of nitrogen and iodine in bioturbated marine sediments. Geochim. Cosmochim. Act. 64, 2751–2763. https://doi.org/10.1016/S0016-7037(00)00400-2.

Auderset, A., Martìnez-García, A., Tiedemann, R., Hasenfratz, P., Eglington, T.I., Schiebel, R., Sigman, D.M., Haug, G.H., 2019. Gulf Stream intensification after the early pliocene shoaling of the Central American Seaway. Earth Planet. Sci. Lett. 520, 268–278. https://doi.org/10.1016/j.epsl.2019.05.022.

Auderset, A., Moretti, S., Taphorn, B., Ebner, P.-R., Kast, E., Wang, X.T., Schiebel, R., Sigman, D.M., Haug, G.H., Martìnez-García, A., 2022. Enhanced ocean oxygenation during cenozoic warm periods. Nature 609, 77–82. https://doi.org/10.1038/s41586-022-05017-0.

Aze, T., Ezard, T.H.G., Purvis, A., Coxall, H.K., Steward, D.R.M., Wade, B.S., Pearson, P. N., 2011. A phylogeny of cenozoic macroperforate planktonic foraminifera from fossil data. Biol. Rev. Camb. Philos. Soc. 86, 900–927. https://doi.org/10.1111/j.1469-185X.2011.00178.x.

Barker, S., Greaves, M., Elderfield, H., 2003. A study of cleaning procedures used for foraminiferal Mg/Ca paleothermometry. Geochem. Geophys. Geosyst. 49 (9), 8407. https://doi.org/10.1029/2003GC000559.

Boscolo-Galazzo, F., Crichton, K.A., Ridgwell, A., Mawbey, E.M., Wade, B.S., Pearson, P. N., 2021. Temperature controls carbon cycling and biological evolution in the ocean twilight zone. Science (1979) 364, 1148–1152. https://doi.org/10.1126/science.abb6643.

Bostock, H.C., Oppdyke, B.N., Williams, M.J.M., 2010. Characterising the intermediate depth waters of the Pacific Ocean using $\delta^{13}C$ and other geochemical tracers. Deep-Sea Res. 1: Oceanogr. Res. Pap. 57, 847–859. https://doi.org/10.1016/j.dsr.2010.04.005.

Branson, O., Read, E., Redfern, S.A.T., Rau, C., Elderfield, H., 2015. Revisiting diagenesis on the Ontong Java Plateau: evidence for authigenic crust precipitation in *globorotalia tumida*. Paleoceanography 30, 1490–1502. https://doi.org/10.1002/2014PA002759.

Breitburg, D., Levin, L.A., Oschlies, A., Grégoire, M., Chavez, F.P., Conley, D.J., Garçon, V., De Nis Gilbert, D., Gutiérrez, K., Isensee, G., Jacinto, G., Limburg, K.E., Montes, I., Naqvi, S.W.A., Pitcher, G.C., Rabalais, N.N., Roman, M.R., Rose, K.A., Seibel, B.A., Telszewksi, M., Yasuhara, M., 2018. Declining oxygen in the global ocean and coastal waters. Science (1979) 359, eeam7240. https://doi.org/10.1126/science.aam7240.

Brown, R.M., Chalk, T.B., Crocker, A.J., Wilson, P.A., Foster, G.L., 2022. Late Miocene cooling coupled to carbon dioxide with pleistocene-like climate sensitivity. Nat. Geosci. 15, 664–670. https://doi.org/10.1038/s41561-022-00982-7.

Busecke, J.J.M., Resplandy, L., Dunne, J.P., 2019. The equatorial undercurrent and the oxygen minimum zone in the Pacific. Geophys. Res. Lett. 46, 6716–6725. https://doi.org/10.1038/s41561-022-00982-7.

Butzin, M., Lohmann, G., Bickert, T., 2011. Miocene ocean circulation inferred from marine carbon cycle modelling combined with benthic isotope records. Paleoceanography 26, PA1203. https://doi.org/10.1029/2009PA001901.

Chance, R., Baker, A.R., Carpenter, L., Jickells, T.D., 2014. The distribution of iodide at the sea surface. Environ. Sci.: Processes Impacts 16, 1841–1859. https://doi.org/10.1039/C4EM00139G.

Chanda, P., Gorski, C.A., Oakes, R.L., Fantle, M.S., 2019. Low temperature stable mineral recrystallization of foraminiferal tests and implications for the fidelity of geochemical proxies. Earth Planet. Sci. Lett. 506, 428–440. https://doi.org/10.1016/j.epsl.2018.11.011.

Cliff, E., Khatiwala, S., Schmittner, A., 2021. Glacial deep ocean deoxygenation driven by biologically mediated air-sea disequilibrium. Nat. Geosci. 14, 43–50. https://doi.org/10.1038/s41561-020-00667-z.

Cutter, G.A., Moffett, J.W., Nielsdóttir, M.C., Sanial, V., 2018. Multiple oxidation state trace elements in suboxic off Peru: in situ redox processes and advective/diffusive horizontal transport. Mar. Chem. 201, 77–89. https://doi.org/10.1016/j.marchem.2018.01.03.

Davis, C.V., Benitez-Nelson, C.R., 2020. Evidence for rapid trace element alteration of planktic foraminiferal shells from the Panama Basin: manganese adsorption during vertical transport. Mar. Micropal. 157, 101872. https://doi.org/10.1016/j.marmicro.2020.101872.

Davis, C.V., Sibert, E.C., Jacobs, P.H., Burls, N., Hull, P.M., 2023. Intermediate water circulation drives distribution of pliocene oxygen minimum zones. Nat. Commun 14 (40). https://doi.org/10.1038/s41467-022-35083-x.

Dekens, P.S., Ravelo, A.C., McCarthy, M.D., 2007. Warm upwelling regions in the pliocene warm period. Paleoceanography 22, PA3211. https://doi.org/10.1029/2006PA001394.

Drury, A.J., Lee, G.P., Gray, W.R., Lyle, M., Westerhold, T., Shevenell, A.E., John, C.M., 2018. Deciphering the state of the late miocene to early pliocene equatorial Pacific. Paleoceanograph. Paleoclimatol. 33, 246–263. https://doi.org/10.1002/2017PA003245.

Evangelinos, D., Etourneau, J., van de Flierdt, T., Crosta, X., Jeandel, C., Flores, J.-A., Harwood, D.M., Valero, L., Ducassou, E., Sauermilch, I., Klocker, A., Cacho, I., Pena, L.D., Kreissig, K., Benoit, M., Belhadj, M., Paredesm, E., Garcia-Solsona, E., López-Quirós, A., Salabarnada, A., Escutia, C., 2024. Late Miocene onset of the

modern Antarctic Circumpolar Current. Nat. Geosci. 17, 165–170. https://doi.org/10.1038/s41561-023-01356-3.
Evans, N., Johnson, E., Taing, A., Schnur, A.A., Chace, P.J., Richards, S., Hardisty, D.S., Moffett, J.W., 2024. More than deoxygenation: linking iodate reduction to nitrogen, iron, and sulfur chemistry in reducing regimes. J. Geophys. Res. Oceans 129. https://doi.org/10.1029/2024JC021013 e2024JC02103.
Farrenkopf, A.M., Luther III, G.M., 2002. Iodine chemistry reflects productivity and denitrification in the Arabian Sea: evidence for flux of dissolved species from sediments of western Indian into the OMZ. Deep-Sea Res. II: Top. Stud. Oceanogr. 48, 2303–2318. https://doi.org/10.1016/S0967-0645(02)00038-3.
Feng, X., Redfern, S.A.T., 2018. Iodate in calcite, aragonite and vaterite $CaCO_3$: insights from first- principles calculations and implications for the I/Ca geochemical proxy. Geochem. Cosmochim. Act. 236, 351–360. https://doi.org/10.1016/j.gca.2018.02.017.
Garcia, H.E., Weathers, K.W., Paver, C.R., Smolyar, I., Boyer, T.P., Locarini, R.A., Zweng, M.M., Mishonov, A.V., Baranova, O.K., Seidov, D., Reagan, J.R., 2019. World Ocean Atlas 2019, volume 3: dissolved oxygen, apparent oxygen utilization, and dissolved oxygen saturation.
Glock, N., Liebetrau, V., Eisenhauer, A., 2014. I/Ca ratios in benthic foraminifera from the Peruvian oxygen minimum zone: analytical methodology and evaluation as a proxy for redox conditions. Biogeosci 11, 7077–7095. https://doi.org/10.5194/bg-11-7077-2014.
Gradstein, F.M., Ogg, J.G., 2012. In: Schmitz, M.D., Ogg, G.M. (Eds.), The Geological Time Scale 2012. Elsevier, Amsterdam, p. 1176.
Groeneveld, J., Henderiks, J., Renema, W., McHugh, C.M., De Vleeschouwer, D., Christensen, B.A., Fulthorpe, C.S., Reuning, L., Gallagher, S.J., Bogus, K., Auer, G., Ishiwa, T., 2017. Australian shelf sediments reveal shifts in miocene Southern Hemisphere westerlies. Sci. Adv. 3, e1602567. https://doi.org/10.1126/sciadv.1602567.
Hardisty, D.S., Lu, Z., Bekker, A., Diamond, C.W., Gill, B.C., Jiang, G., Kah, L.C., Knoll, A. H., Loyd, S.J., Osburn, M.R., Planavsky, N.J., Wang, C., Zhou, X., Lyons, T.W., 2017. Perspectives on proterozoic surface ocean redox from iodine contents in ancient and recent carbonate. Earth Planet. Sci. Lett. 463, 159–170. https://doi.org/10.1016/j.epsl.2017.01.032.
Hardisty, D.S., Horner, T.J., Evans, N., Moriyasu, R., Babbin, A.R., Wankel, S.D., Moffett, J.W., Nielsen, S.G., 2021. Limited iodate reduction in shipboard seawater incubations from the Eastern Tropical North Pacific oxygen deficient zone. Earth. Planet. Sci. Lett. 554, 116676. https://doi.org/10.1016/j.epsl.2020.116676.
Helly, J.J., Levin, A., 2004. Global distribution of naturally occurring marine hypoxia on continental margins. Deep Sea Res. Part 1 Oceanogr. 51, 1159–1168. https://doi.org/10.1016/j.dsr.2004.03.009.
Herbert, T.D., Lawrence, K.T., Tzanova, A., Cleaveland Peterson, L., Caballero-Gill, R., Kelly, C.S., 2016. Late Miocene global cooling and the rise of modern ecosystems. Nat. Geosci. 9, 843–847. https://doi.org/10.1038/ngeo2813.
Hess, A.V., Auderset, A., Rosenthal, Y., Miller, K.G., Zhou, X., Sigman, D.M., Martínez-García, A., 2023. A well-oxygenated eastern tropical Pacific during the warm Miocene. Nature 619, 521–525. https://doi.org/10.1038/s41586-023-06104-6.
Holbourn, A., Kuhnt, W., Frank, M., Haley, B.A., 2013. Changes in Pacific Ocean circulation following the Miocene onset of permanent Antarctic ice cover. Earth Planet. Sci. Lett. 356, 38–50. https://doi.org/10.1016/j.epsl.2013.01.020.
Holbourn, A., Kuhnt, W., Kochhann, K.G.D., Matsuzaki, K.M., Andersen, N., 2022. Middle Miocene climate-carbon cycle dynamics: keys for understanding future trends on a warmer Earth? Geol. Soc. Am. 556, 93–111. https://doi.org/10.1130/2022.2556(05).
Hoogakker, B.A.A., Lu, Z., Umling, N., Jones, L., Zhou, X., Rickaby, R.E.M., Thunell, R., Cartapanis, O., Galbraith, E.D., 2018. Glacial expansion of oxygen-depleted seawater in the eastern tropical Pacific. Nature 562, 410–413. https://doi.org/10.1038/s41586-018-0589-x.
Jaccard, S.L., Galbraith, E.D., 2012. Large climate-driven changes of oceanic oxygen concentrations during the last deglaciation. Nat. Geosci. 5, 151–156. https://doi.org/10.1038/ngeo1352.
Jacobel, A.W., Anderson, R.F., Jaccard, S.L., McManus, J.F., Pavia, F.J., Winckler, G., 2020. Deep Pacific storage of respired carbon during the last ice age: perspectives from bottom water oxygen reconstructions. Quat. Sci. Rev. 230, 106065. https://doi.org/10.1016/j.quascirev.2019.106065.
Jaramillo, C., Montes, C., Cardona, A., Silvestro, D., Antonelli, A., Bacon, C.D., 2017. Comment (1) on "Formation of Isthmus of Panama" by O'Dea et al. Sci. Adv. 3, e1602321. https://doi.org/10.1126/sciadv.1602321.
Karas, C., Nürnberg, D., Bahr, A., Groeneveld, J., Herrle, J.O., Tiedemann, R., deMenocal, P.B., 2017. Pliocene oceanic seaways and global climate. Sci. Rep. 7, 39842. https://doi.org/10.1038/srep39842.
Karstensen, J., Stramma, L., Visbeck, M., 2008. Oxygen minimum zones in the eastern tropical Atlantic and Pacific Oceans. Prog. Oceanograph. 77, 331–350. https://doi.org/10.1016/j.pocean.2007.05.009.
Keeling, R.F., Körtzinger, A., Gruber, N., 2010. Ocean deoxygenation in a warming world. Annu. Rev. Mar. Sci. 2, 199–229. https://doi.org/10.1146/annurev.marine.010908.163855.
Kessler, W.S., 2006. The circulation of the eastern tropical Pacific: a review. Prog. Oceanograph. 69, 181–217. https://doi.org/10.1016/j.pocean.2006.03.009.
Khon, V.C., Hoogakker, B.A.A., Schneider, B., Segschneider, J., Park, W., 2023. Effect of an open Central American Seaway on ocean circulation and the Oxygen Minimum Zone in the tropical Pacific from model simulations. Geophys. Res. Lett. 50, e2023GL103728. https://doi.org/10.1029/2023GL103728.
Kirillova, V., Osborne, A.H., Störling, T., Frank, M., 2019. Miocene restriction of the Pacific North Atlantic throughflow strengthened Atlantic overturning circulation. Nat. Commun 10. https://doi.org/10.1038/s41467-019-12034-7.
Kroenke, L.W., Berger, W.H., Janecek, T.R., et al., 1991. In: Proc. ODP Init. Reports, p. 130.
Lau, K.V., Hardisty, D.S., 2022. Modelling the impacts of diagenesis on carbonate paleoredox proxies. Geochim. Cosmochim. Act. 337, 123–129. https://doi.org/10.1016/j.gca.2022.09.021.
Lear, C.H., Rosenthal, Y., Wright, J.D., 2003. The closing of a seaway: ocean water masses and global climate change. Earth Planet. Sci. Lett. 210, 425–436. https://doi.org/10.1016/S0012-821X(03)00164-X.
Leutert, T.J., Auderset, A., Martínez-García, A., Modestou, S., Meckler, A.N., 2020. Coupled Southern Ocean cooling and Antarctic ice sheet expansion during the middle Miocene. Nat. Geosci. 13, 634–639. https://doi.org/10.1038/s41561-020-0623-0.
Li, G., Cheng, J., Zhu, J., Trenberth, K.E., Mann, M.E., Abraham, J.P., 2020. Increasing ocean stratification over the past half-century. Nat. Clim. Chang. 10, 1116–1123. https://doi.org/10.1038/s41558-020-00918-2.
Li, Z., Zhang, Y.G., Torres, M., Mills, B.J.W., 2023. Neogene burial of organic carbon in the global ocean. Nature 613, 90–95. https://doi.org/10.1038/s41586-022-05413-6.
Lu, W., Rickaby, R.E.M., Hoogakker, B.A.A., Rathburn, A.E., Burkett, A.M., Dickson, A.J., Martínez-Méndez, G., Hillenbrand, C.-D., Zhou, Z., Thomas, E., 2020a. I/Ca in epifaunal benthic foraminifera: a semi-quantitative proxy for bottom water oxygen in a multi-proxy compilation for glacial ocean deoxygenation. Earth. Planet. Sci. Lett. 533, 116055. https://doi.org/10.1016/j.epsl.2019.116055.
Lu, W., Dickson, A.J., Thomas, E., Rickaby, R.E.M., Chapman, P., Lu, Z., 2020b. Refining the planktic foraminiferal I/Ca proxy: results from the Southeast Atlantic Ocean. Geochim. Cosmochim. Act. 287, 318–327. https://doi.org/10.1016/j.gca.2019.10.025.
Lu, Z., Hoogakker, B.A.A., Hillenbrand, C.-D., Zhou, X., Thomas, E., Gutchess, K.M., Lu, W., Jones, L., Rickaby, R.E.M., 2016. Oxygen depletion recorded in upper waters of the glacial Southern Ocean. Nat. Commun 7, 11146. https://doi.org/10.1038/ncomms11146.
Lu, Z., Thomas, E., Rickaby, R.E.M., Lu, W., Prow, A.N., 2023. Commentary: planktic foraminifera iodine/calcium ratios from plankton tows. Front. Mar. Sci. 10, 1221835. https://doi.org/10.3389/fmars.2023.1221835.
Lyle, M., Baldauf, J., 2015. Biogenic sediment regimes in the Neogene equatorial Pacific, IODP Site U1338: burial, production, and diatom community. Palaeogeograph. Palaeoclimatol. Palaeoecol. 433, 106–128. https://doi.org/10.1016/j.palaeo.2015.04.001.
Lyle, M., Drury, A.J., Tian, J., Wilkens, R., Westerhold, T., 2019. Late Miocene to Holocene high- resolution eastern equatorial Pacific carbonate records: stratigraphy linked by dissolution and paleoproductivity. Clim. Past. 15, 1715–1739. https://doi.org/10.5194/cp-15-1715-2019.
Martínez-Botí, M.A., Marino, G., Foster, G.L., Ziveri, P., Henehan, M.J., Rae, J.W.B., Mortyn, P.G., Vance, D., 2015. Boron isotope evidence for oceanic carbon dioxide leakage during the last deglaciation. Nature 528, 219–222. https://doi.org/10.1038/nature14155.
Mix, A.C., Tiedemann, R., Blum, P., et al., 2003. In: Proc. ODP, Init Reports, p. 202.
Moriyasu, R., Evans, N., Bolster, K.M., Hardisty, D.S., Moffett, J.W., 2020. The distribution and redox speciation of iodine in the Eastern Tropical North Pacific Ocean. Global Biogeochem. Cycles. 34, e2019GB006302. https://doi.org/10.1029/2019GB006302.
Müller, R.D., Cannon, J., Qin, X., Watson, R.J., Gurnis, M., Williams, S., Pfaffelmoser, T., Seton, M., Russell, S.H.J., Zahirovic, S., 2018. Gplates: building a virtual Earth through deep time. Geochem. Geophys. Geosyst. 19, 2243–2261. https://doi.org/10.1029/2018GC007584.
Nisancioglu, K.H., Raymo, M.E., Stone, P.H., 2003. Reorganization of Miocene deep-water circulation in response to the shoaling of the Central American Seaway. Paleoceanography 18, 1006. https://doi.org/10.1029/2002PA000767.
Newkirk, D.R., Martin, E.E., 2009. Circulation through the Central American seaway during the miocene carbonate crash. Geology. 37, 87–90. https://doi.org/10.1130/G25193A.1.
O'Dea, A., Lessios, H.A., Coates, A.G., Eytan, R.I., Restrepo-Moreno, S.A., Cione, A.L., Collins, L.S., De Quiroz, A., Farris, D.W., Norris, R.D., Stallard, R.F., Woodburne, M. O., Aguilera, O., Aubry, M.-P., Beggren, W.A., Budd, A.F., Cozzuol, M.A., Coppard, S. E., Dueque-Caro, H., Finnegan, S., Gasparini, G.M., Grossman, E.L., Johnson, K.G., Keigwin, L.D., Knowlton, N., Leigh, E.G., Leonard-Pingel, J.S., Marko, P.B., Pyenson, N.D., Rachello- Dolmen, P.G., Soibelzon, E., Soibelzon, L., Todd, J.A., Vermeij, G.J., Jackson, J.B.C., 2016. Formation of the isthmus of Panama. Sci. Adv. 2, e1600883. https://doi.org/10.1126/sciadv.1600883.
Osborne, A.H., Newkirk, D.R., Groeneveld, J., Martin, E.E., Tiedemann, R., Frank, M., 2014. The seawater neodymium and lead isotope record of the final stages of the Central American Seaway closure. Paleoceanograph. Paleoclimatol. 29, 715–729. https://doi.org/10.1002/2014PA002676.
Oschlies, A.A., 2021. A committed fourfold increase in ocean oxygen loss. Nat. Commun 12, 2307. https://doi.org/10.1038/s41467-021-22584-4.
Pennington, J.T., Mahoney, K.L., Kuwahara, V.S., Kolber, D.D., Calienes, R., Chavez, F.P., 2006. Primary production in the eastern tropical Pacific: a review. Prog. Oceanograph. 69, 285–317. https://doi.org/10.1016/j.pocean.2006.03.012.
Pälike, H., Nishi, H., Lyle, M., Raffi, I., Gamage, K., Klaus, A., 2010. In: Proc. Integrated Ocean Drilling Program 320/321.
Raymo, M.E., 1994. The initiation of Northern Hemisphere glaciation. Annu. Rev. Earth Planet. Sci. 22, 353–383. https://doi.org/10.1146/annurev.ea.22.050194.002033.
Ronge, T.A., Frische, M., Fietzke, J., Stephens, A.L., Bostock, H., Tiedemann, R., 2021. Southern Ocean contribution to both steps in deglacial atmospheric CO_2 rise. Sci. Rep. 11, 22117. https://doi.org/10.1038/s41598-021-01657-w.

Rue, E.L., Smith, G.J., Cutter, G.A., Bruland, K.W., 1997. The response of trace element redox couples to suboxic conditions in the water column. Deep Sea Res. Part I. 44, 113–134. https://doi.org/10.1016/S0967-0637(96)00088-X.

Shankle, M.G., Burls, N.J., Fedorov, A.V., Thomas, M.D., Liu, W., Penman, D.E., Ford, H. L., Jacobs, P.H., Planavsky, N.J., Hull, P.M., 2021. Pliocene decoupling of equatorial Pacific temperature and pH gradients. Nature 598, 457–461. https://doi.org/10.1038/s41586-021-03884-7.

Shuttleworth, R., Bostock, H.C., Chalk, T.B., Calvo, E., Jaccard, S.L., Pelejero, C., Martínez- García, A., Foster, G.L., 2021. Early deglacial CO_2 release from the Sub-Antarctic Atlantic and Pacific Oceans. Earth. Planet. Sci. Lett. 554, 1166449. https://doi.org/10.1016/j.epsl.2020.116649.

Skinner, L., McCave, I.N., Carter, L., Fallon, S., Scrivner, A.E., Primeau, F., 2015. Reduced ventilation and enhanced magnitude of the deep Pacific carbon pool during the last glacial period. Earth. Planet. Sci. Lett. 411, 45–52. https://doi.org/10.1016/j.epsl.2014.11.024.

Steph, S., Tiedemann, R., Prange, M., Groeneveld, J., Nürnberg, D., Reuning, L., Schulz, M., Haug, G.H., 2006. Changes in Caribbean surface hydrography during the pliocene shoaling of the Central American Seaway. Paleoceanography 21, PA4221. https://doi.org/10.1029/2004PA001092.

Takahashi, T., Sutherland, S.C., Sweeney, C., Poisson, A., Metzl, N., Tilbrook, B., Bates, N., Wanninkhof, R., Feely, R.A., Sabine, C., Olafsson, J., Nojiri, Y., 2009. Global sea-air CO_2 flux based on climatological surface ocean pCO_2, and seasonal biological and temperature effects. Deep Sea Res. Part II. 56, 554–577. https://doi.org/10.1016/S0967-0645(02)00003-6.

Talley, L.D., Pickard, G.L., Emery, W.J., Swift, J.H., 2011. Descriptive Physical Oceanography, An Introduction, 6th ed. Elsevier.

The Cenozoic CO2 Proxy Integration Project (CenCO2PIP) Consortium, 2023. Toward a cenozoic history of atmospheric CO2. Science (1979) 382, eadi5177. https://doi.org/10.1126/science.adi5177.

Tsuchiya, M., Lukas, R., Fine, R.A., Firing, E., Lindstrom, E., 1989. Source waters of the Pacific Equatorial Undercurrent. Prog. Oceanograph. 23, 101–147. https://doi.org/10.1016/0079-6611(89)90012-8.

Wang, X.T., Wang, Y., Auderset, A., Sigman, D.M., Ren, H., Martínez-García, A., Haug, G. H., Su, Z., Zhang, Y.G., Rasmussen, B., Sessions, A.L., Fischer, W.W., 2022. Oceanic nutrient rise and the late miocene inception of Pacific oxygen-deficient zones. Proc. Natl. Acad. Sci. USA 119, e2204986119. https://doi.org/10.1073/pnas.2204986119.

Winkelbauer, H., Cordova-Rodriguez, K., Reyes-Macaya, D., Scott, J., Glock, N., Lu, Z., Hamilton, E., Chenery, S., Holdship, P., Dormon, C., Hoogakker, B., 2021. Foraminifera iodine to calcium ratios: approach and cleaning. Geochem. Geophys. Geosystem. 22, e2021GC009811. https://doi.org/10.1029/2021GC009811.

Winkelbauer, H.A., Hoogakker, B.A.A., Chance, R.J., Davis, C.V., Anthony, C.J., Bischoff, J., Carpenter, L.C., Chenery, S.R.N., Hamilton, E.M., Holdship, P., Peck, V. L., Poulton, A.J., Stinchcombe, M.C., Wishner, K.F., 2023. Planktic foraminifera iodine/calcium ratios from plankton tows. Front. Mar. Sci. 10, 1095570. https://doi.org/10.3389/fmars.2023.1095570.

Woodhouse, A., Swain, A., Fagan, W.F., Frass, A.J., Lowery, C.M., 2023. Late Cenozoic cooling restructured global marine plankton communities. Nature 614, 713–718. https://doi.org/10.1038/s41586-023-05694-5.

Zhang, Y.G., Pagani, M., Liu, Z., 2014. A 12-million-year temperature history of the tropical Pacific Ocean. Science (1979) 344, 84–87. https://doi.org/10.1126/science.1246172.

Zhang, Z., Nisanciouglu, K.H., Flatøy, F., Bentsen, M., Bethke, I., Wang, H., 2011. Tropical seaways played a more important role than high latitude seaways in cenozoic cooling. Clim. Past. 7, 801–813. https://doi.org/10.5194/cp-7-801-2011.

Zhou, X., Thomas, E., Rickaby, R.E.M., Winguth, A.M.E., Lu, Z., 2014. I/Ca evidence for upper ocean deoxygenation during the PETM. Paleoceanograph. Paleoclimatol. 29, 964–975. https://doi.org/10.1002/2014PA002702.

Zhou, X., Jenkyns, H.C., Owens, J.D., Junium, C.K., Zheng, X.-Y., Sageman, B.B., Hardisty, D.S., Lyons, T.W., Ridgwell, A., Lu, Z., 2015. Upper ocean oxygenation dynamics from I/Ca ratios during the cenomanian-turonian OAE 2. Paleoceanography 30, 510–526. https://doi.org/10.1002/2014PA002741.